Real-Time Magnetic Resonance Imaging–Guided Stenting of Aortic Coarctation With Commercially Available Catheter Devices in Swine

Amish N. Raval, MD, **James D. Telep, MD**[*], **Michael A. Guttman, MSc**[*], **Cengizhan Ozturk, MD, PhD**, **Michael Jones, MD**, **Richard B. Thompson, PhD**, **Victor J. Wright, BS**, **William H. Schenke, BS**, **Ranil DeSilva, MBBS, PhD**, **Ronnier J. Aviles, MD**, **Venkatesh K. Raman, MD**, **Michael C. Slack, MD**, and **Robert J. Lederman, MD**

From the Cardiovascular Branch (A.N.R., J.D.T., C.O., M.J., V.K.R., V.J.W., W.H.S., R.D.S., R.J.A., R.J.L.) and the Laboratory of Cardiac Energetics (M.A.G., R.B.T., E.R.M.), Division of Intramural Research, National Heart Lung and Blood Institute, National Institutes of Health, Bethesda, Md; Division of Pediatric Cardiology (J.D.T., M.C.S.), Children's National Medical Center, Washington, DC; and Department of Biomedical Engineering (R.B.T.), University of Alberta, Edmonton, Canada.

Abstract

Background—Real-time MR imaging (rtMRI) is now technically capable of guiding catheter-based cardiovascular interventions. Compared with x-ray, rtMRI offers superior tissue imaging in any orientation without ionizing radiation. Translation to clinical trials has awaited the availability of clinical-grade catheter devices that are both MRI visible and safe. We report a preclinical safety and feasibility study of rtMRI-guided stenting in a porcine model of aortic coarctation using only commercially available catheter devices.

Method and Results—Coarctation stenting was performed wholly under rtMRI guidance in 13 swine. rtMRI permitted procedure planning, device tracking, and accurate stent deployment. "Active" guidewires, incorporating MRI antennas, improved device visualization compared with unmodified "passive" nitinol guidewires and shortened procedure time (26±11 versus 106±42 minutes; $P = 0.008$). Follow-up catheterization and necropsy showed accurate stent deployment, durable gradient reduction, and appropriate neointimal formation. MRI immediately identified aortic rupture when oversized devices were tested.

Conclusions—This experience demonstrates preclinical safety and feasibility of rtMRI-guided aortic coarctation stenting using commercially available catheter devices. Patients may benefit from rtMRI in the future because of combined device and tissue imaging, freedom from ionizing radiation, and the ability to identify serious complications promptly.

Endovascular stenting effectively relieves focal native and recurrent aortic coarctation in children and adults.[1-3] X-ray fluoroscopy (XRF) is used in these procedures with intermittent boluses of iodinated radiocontrast to define anatomic targets and to guide devices. This

Correspondence to Robert J. Lederman, MD, Cardiovascular Branch, Division of Intramural Research, National Heart, Lung, and Blood Institute, National Institutes of Health, Bldg 10, Room 2c713, MSC 1538, Bethesda, MD 20892–1538. E-mail lederman@nih.gov.
[*]Drs Raval and Telep contributed equally to this work.

approach is limited because XRF does not visualize soft tissue, lacks depth perspective, and exposes patients to ionizing radiation.

MRI displays soft tissue detail in any spatial orientation, requires no ionizing radiation, and can provide hemodynamic information. Real-time MRI (rtMRI) is now technically feasible and has enabled transcatheter treatment of congenital[4–7] and acquired[8–20] cardiovascular disease in animal models and humans.

Razavi and colleagues[21] demonstrated safety and feasibility of cardiovascular catheterization in children and adults using a combined XRF and MRI suite. MRI-guided therapeutic human procedures will require conspicuous clinical-grade catheter devices. Our aim was to test the safety and feasibility of wholly MRI-guided stenting of aortic coarctation in swine using commercially available clinical devices. Specifically, we hypothesize that rtMRI can (1) provide safe and accurate device navigation, positioning, and deployment; (2) provide immediate preprocedural and postprocedural anatomic and hemodynamic assessment; (3) provide early recognition of significant complications; and (4) be conducted with catheter devices commercially available in the United States.

Methods

Animal Model of Aortic Coarctation

Animal protocols were approved by the National Heart, Lung, and Blood Institute (NHLBI) Animal Care and Use Committee. A surgical model of postductal aortic coarctation[22] was created in 13 juvenile NIH miniswine (23 to 38 kg). After induction with tilet-amine/ zolazepam, xylazine, and inhaled isoflurane, the aorta was exposed via the second left intercostal space. A side clamp was applied to the aorta distal to the ligamentum arteriosum, and an ellipse was excised laterally to encompass two thirds of the aortic circumference. The free edges of the aorta were reapposed and buttressed circumferentially with absorbable suture. A target gradient of 30 to 80 mm Hg was confirmed by direct needle puncture, with the expectation that the gradient would diminish during convalescence. In our experience, higher acute gradients result in early heart failure and death. Catheter experiments were delayed at least 4 weeks after surgery to allow fibrosis of the coarctation lesion. Similar anesthesia was used for transcatheter experiments. Animals received oral clopidogrel and aspirin before and after catheter procedures. After arterial access, heparin 120 U/kg IV was administered and supplemented as needed. Prophylactic cefazolin was administered for survival procedures.

X-Ray/MRI Intervention Suite

The NHLBI cardiovascular x-ray/MRI intervention suite consists of independently operating MRI and XRF systems (Sonata 1.5T and Axiom Artis FC, Siemens).[23] They are separated by sliding doors containing both x-ray and radiofrequency shields. For combined procedures, the doors are opened, and the x-ray pedestal is translated on motorized rails (Miyabe, Siemens) to transfer a patient between the XRF and MRI systems. Real-time images were displayed in the laboratory with radiofrequency-shielded LCD projectors. The suite was equipped with an MR-compatible monitoring system providing instantaneous oximetry, dual-channel invasive blood pressure, and ECG display (Magnitude CV, In-Vivo Research). The staff communicated using a custom sound suppression system incorporating directional optical microphones and radiofrequency-filtered headsets (Phone-Or and Magnacoustics). MRI coils included standard 6-channel torso and spine phased-array surface coils (Siemens) and intravascular guidewire coils (described below) connected on separate MRI receiver channels.

MRI data were transferred during scanning via Gigabit Ethernet to an external computer (Dual CPU Pentium 4 running Linux, ASL, Inc) for real-time image reconstruction and interactive

scan control.[24] Acquisition, reconstruction, and display of each frame was completed within 250 ms. Images created from intravascular guide-wire receiver coils (see below) were color highlighted for enhanced visibility. To sharpen their color profiles and suppress noise, the signal intensity values from these intravascular coils were squared before blending with surface coil images. The imaging frame rate could be accelerated using view sharing between even and odd echoes. Magnetization preparation pulses such as nonselective water or fat saturation could be toggled on/off during imaging. ECG gating could be toggled on/off to "freeze" motion, and temporal image filtering (averaging) could be applied interactively to increase signal-to-noise ratio. Multiple oblique slices could be acquired simultaneously, moved interactively, or omitted individually as desired. To visualize the complex interrelation of anatomy, function, and catheter/stent position, a 3D rendering was used to display all or selected slices at their respective spatial positions.[25] Noteworthy anatomic locations could be marked in 3D on the computer display.

MRI Study

Coarctation geometry was delineated before and after stenting with gated "black-blood" double-inversion-recovery fast-spin-echo (DIR-FSE) MRI in both long- and short-axis stacks. Typical imaging parameters were as follows: repetition time (TR), 1350 ms; echo time (TE), 960 ms; field of view (FOV), 320×225 mm; averages, 4; bandwidth, 130 Hz per pixel; slice thickness, 3 mm; and matrix, 384×265. Contrast-enhanced 3D MR angiography (CE-MRA) used intravenous gadopentetate dimeglumine (DTPA; Magnevist, Berlex) 0.1 mmol/kg and spoiled gradient echo with TR/TE of 3.72/1.44 ms, flip angle of 25°, FOV of 30×30×10 cm, bandwidth of 742 Hz per pixel, matrix of 512×512×72. Through-plane peak instantaneous velocities were sampled using free-breathing 2D phase-contrast MRI (PC-MRI). Preliminary long- and short-axis PC-MRI and steady-state free precession (SSFP) in this animal model demonstrated uniform flow acceleration beginning in the narrowest coarctation lumen, with a vena contracta that tapered 10 mm distally. Orthogonal slices were positioned within the smallest coarctation lumen before stenting and subsequently 5 mm beyond the stent edge. Flow analyses were performed with Argus Flow software (Siemens). The corresponding peak gradients were calculated with a modified Bernoulli formula: $\Delta pressure = 4\times(peak\ velocity)^2$. Typical PCI-MRI parameters were as follows: TR/TE, 33/3 ms; flip angle, 30°; FOV, 28 cm; velocity encoding, 350 cm/s; bandwidth, 1528 Hz per pixel; matrix, 256×256; and slice thickness, 5 mm. PC-MRI data were reformatted as color flow maps with Matlab (Mathworks).

Catheter manipulations were guided by real-time SSFP.[9] With echo sharing, this generated 8 frames per second. Typical imaging parameters were as follows: TR/TE, 2.8/1.4 ms; flip angle, 60°; bandwidth, 800 Hz per pixel; matrix, 192×108; and FOV, 32×24 cm, generating 1.7×2.2×6-mm voxels.

For each procedure, interactive interventional imaging began with slices selected to show the aorta and left subclavian artery origin. Multiple axial views were obtained through the middle of the coarctation, the subclavian origin, and distal to the coarctation at the level of the highest normal descending aorta. Reference aortic lumen caliber represented the average of measurements at the subclavian and diaphragmatic levels measured with DIR-FSE MRI.

Invasive Devices

Catheter devices were selected for safety and compatibility in an MRI environment. The Intercept guidewire (Surgi-Vision) has 510(k) Food and Drug Administration (FDA) marketing clearance for invasive MRI. In manufacturer phantom tests, the guidewire was associated with trivial heating of a vascular phantom (<0.3°C) over 10 minutes of continuous fast spoiled-gradient-echo scanning with a high flip angle (personal communication with A.C. Lardo, 2001). For comparison, in 5 animals, a standard 0.035-in Teflon-coated nitinol

guidewire (Glidewire, Terumo/Boston Scientific) was used for "passive" device delivery, even though it is known to heat inductively during MRI.[26] Platinum-iridium stents (Cheatham Z-stent, NuMed Inc) cause only modest shielding artifacts under MRI[27] and are commercially available with FDA Humanitarian Device Exemptions. The stents were hand crimped onto an 8F balloon-in-balloon dilatation catheter (BIB, NuMed) sized 1.2:1 to the reference aorta caliber. An alternative prototype cobalt-nickel-chromium alloy (MP35N) stent was used in 1 animal (Medtronic).

X-Ray Control Procedures

A 10F introducer sheath was inserted into a femoral artery. Pressure gradients were measured across the coarctation before and after isoproterenol $0.2\,\mu g \cdot kg^{-1} \cdot min^{-1}$ infusion. X-ray digital subtraction angiography was performed and devices were removed before the animals were transported into the MRI with continuous hemodynamic monitoring. After rtMRI-guided stent delivery, XRF angiographic and hemodynamic examinations were repeated.

Stent Delivery

MRI SSFP localizer images were obtained as described above. Before the interventional procedure began, the lesion and key anatomic features such as the margins of the coarctation lesion and the ostium of the subclavian artery were marked under rtMRI on the 3D-rendered image. The stent-mounted balloon was introduced through the sheath over the Surgi-Vision guidewire. Before crossing the coarctation, the balloon was filled with a small volume of Gd-DTPA (5 mmol/L) to create small "dumbbells" that secure the stent and enhance MRI visibility. Stents were deployed at nominal pressure while simultaneously imaging the balloon and aortic wall. Procedure time was recorded as the time from the first to last rtMRI scan sequence.

Intentional Aortic Rupture

In an effort to detect focal aortic rupture or dissection, deliberately oversized balloons were employed in 4 additional experiments. Hand-crimped stents were deployed at or near burst pressure during continuous rtMRI observation. Immediately afterward, DIR-FSE MRI exams were repeated.

Statistical Analysis

Continuous parameters were reported as mean±SD and were compared by use of Student *t* test.

Results

Coarctation Stenting

Coarctation was created in 13 animals weighing 31.8±5.4 kg. Before stenting, the peak-to-peak catheter gradient was 17±8 mm Hg at rest and 34±18 mm Hg after isoproterenol. The peak instantaneous resting gradient by PC-MRI was 24±7 mm Hg. Figure 1 shows the coarctation using DIR-FSE, CE-MRA, and radiocontrast before (Figure 1A through 1C) and after (Figure 1D through 1F) stenting. The mean reference aortic caliber was 12±1 mm. The mean minimum lumen diameter of the coarctation was 5±1 mm, and the mean stent delivery balloon was 14±1 mm.

Stent delivery over active guidewire receiver coils significantly improved device visibility compared with passive nitinol guidewires (Figure 2). The passive platinum and MP35N stents themselves were visualized under rtMRI as signal voids. The active guidewires easily traversed the model coarctation and were positioned in the left subclavian artery through rtMRI. Procedures using passive nitinol guidewires required significantly more time (106±42 versus 26±11 minutes; *P*=0.008) and effort to position because of their poor visibility.

The custom rtMRI user environment facilitated stent positioning and deployment. Particularly useful features included color highlighting of signal from active guidewire coils and interleaved acquisition of multiple planes combined with online 3D rendering. Virtual markers indicating important coarctation landmarks, positioned on the computer display, also proved very helpful in positioning the delivery system.

Stents were successfully deployed in all 13 animals. A typical stent deployment sequence is depicted in Figure 3. Both platinum and MP35N stents in this caliber and thickness created shielding artifacts obscuring the underlying aortic lumen with SSFP and CE-MRA sequences. These artifacts were not evident with DIR-FSE images (Figure 1D). Stent struts were adequately apposed to the aortic wall in all animals by MRI and XRF.

After stenting, the peak instantaneous gradient across the coarctation was reduced to 8±7 mm Hg with PC-MRI and peak-to-peak systolic gradient to 4±3 mm Hg using catheters (both *P*<0.01 versus baseline). This hemodynamic information was depicted graphically with color maps of blood velocity (Figure 4). The mean minimum lumen diameter on FSE images after stenting was 11±1 mm.

Immediate postprocedure necropsy on 5 animals showed appropriate stent apposition with no visible evidence of thermal injury or thrombus.

Complications

There was no significant whole-animal heating (maximum change of transrectal temperature during the procedure, −0.3±1.1°C). No thrombus adherent to interventional devices during routine catheter exchanges was evident.

In 1 animal early in this experience, a stent was inadvertently displaced inferiorly into the descending aorta by an entangled Teflon-nitinol guidewire that was visualized passively. In this animal, the balloon:reference diameter was 0.9:1 because of inventory limitations. The stent was redeployed in the descending aorta, and another was successfully deployed across the coarctation.

An unintentional focal aortic rupture was created in 1 animal during stent deployment with an oversized balloon (balloon:artery ratio, 1.3:1). The rupture was immediately visible under rtMRI and verified by CE-MRA (Figure 5). No special intervention was offered the animal, which died 3 hours later. Subsequent necropsy showed coarctation suture line disruption.

Intentional Aortic Rupture

Intentional balloon overdilatation to the point of aortic rupture was performed in 4 additional animals. Each was characterized by expanding extramural hematoma along the posterolateral aorta corresponding to the coarctation suture line. This extravasation was immediately evident under rt-MRI and DIR-FSE (Figure 6).

Follow-Up

Four animals were studied 96±40 days after coarctation stenting. The mean follow-up systolic peak-to-peak catheter gradient was 0±0 mm Hg, and the peak instantaneous phase-contrast gradient was 4±1 mm Hg. The mean minimal lumen diameter was 10.5±1 mm; the mean reference aorta diameter was 11±1 mm. Necropsy revealed at least partial neointimal coverage of the stent (Figure 7). There was no necropsy evidence of remote subclavian, aortic, or iliac intimal fibrosis that might represent thermal injury from the guidewire.

Discussion

This experience suggests that wholly MRI-guided aortic coarctation stenting is safe and feasible in an animal model. MRI has the unique advantage of imaging tissue and lumen at the same time as device manipulation. These preclinical experiments were conducted in a clinical laboratory with commercial devices either approved for clinical use or available under humanitarian device exemption from the US FDA. rtMRI provided feedback during stent positioning and deployment, anatomic imaging of stent apposition to the target aortic wall, hemodynamic corroboration of successful stent delivery, and identification of aortic mural disruption in 1 case of unintentional rupture. This approach to coarctation stenting is attractive because of its freedom from ionizing radiation, its continuous display of tissue-device interaction, and its ability to provide immediate evidence of serious complications such as aortic rupture.

Aortic coarctation is common and accounts for 8% to 11% of congenital cardiovascular abnormalities.[28] Surgical repair options include end-to-end reapposition, interposition graft, and patch aortoplasty. Although these can be accomplished with low mortality, serious complications, including phrenic and recurrent laryngeal nerve injury, reactive hypertension, spinal cord ischemia/infarction,[29] and restenosis, still occur.[30] Simple balloon angioplasty is a minimally invasive alternative to surgical repair; however, it is associated with recoil, dissection, aneurysm formation, and late restenosis.[31] Percutaneous stenting is attractive for focal de novo and postsurgical recoarctation[2,3] because it leads to less dissection, restenosis, and late aneurysm formation.[2,3,32,33] Aortic rupture is an uncommon but reported catastrophic complication of coarctation stenting.[3,34,35] Although used extensively, XRF is not ideally suited to guide these procedures because of ionizing radiation exposure and tissue imaging limitations.

Children may be particularly sensitive to x-ray radiation.[36–40] Two historical linkage analyses suggest no additional cancer risk from pediatric cardiac catheterization[41,42]; however, the weight of available evidence indicates increased lifetime cancer risk after x-ray exposure.[37–39,43–46] Therapeutic endovascular procedures are now common and require longer fluoroscopy time than diagnostic catheterization.[45,47–49] Children with congenital cardiovascular disease, including aortic coarctation, often undergo multiple XRF procedures and therefore have greater cumulative radiation exposure. Radiation-sparing procedural guidance with MRI would be attractive.

High-resolution noninvasive MRI is commonly performed for diagnosis and postprocedure surveillance of aortic coarctation.[50,51] In this study, we use MRI with lower spatial resolution but adequate temporal resolution to guide the actual therapeutic procedure. Furthermore, MRI yields anatomic information superior to XRF in any orientation, which is especially attractive in patients with complex 3D coarctation morphology. MRI also can provide spatially resolved hemodynamic information such as blood velocity during the procedure.[52] Adjunctive color-flow mapping may offer a useful "quick glance" at lesion physiology to guide further procedure conduct. Intraprocedural transesophageal or intravascular ultrasound is unable to resolve aortic adventitia or provide orientation-independent anatomic information. Although beyond the scope of this investigation, sophisticated MRI techniques are available to characterize aortic wall stiffness, distensibility, and compliance; these techniques may prove clinically valuable in planning and follow-up of coarctation treatments in the future and are perhaps best studied in humans. In our study, rtMRI provided immediate feedback on serious complications such as aortic perforation. This may provide an additional clinical margin of safety by expediting emergency treatment.

This experience is limited by the simple animal model of aortic coarctation, which is neither geometrically complex nor anatomically severe. The utility of rtMRI remains untested in tortuous, eccentric, and severe coarctation lesions; however, the spatial detail offered by MRI may prove useful compared with XRF. All intentional ruptures were found along the surgical suture line, whereas catastrophic clinical perforations and dissections are less predictable.

The NHLBI x-ray/MRI suite is designed to handle and monitor patients during rtMRI in a manner comparable to conventional XRF interventional laboratories. This configuration provides XRF as an emergency bailout modality should rtMRI systems fail. All catheter systems we used for rtMRI also are suitable for XRF. During MRI scanning, radiofrequency energy deposition on long conductive devices such as guidewires may cause heating.[27,53] We used an FDA-approved active guidewire coil designed to prevent heating by decoupling the device during radiofrequency excitation. This study shows a significant improvement in visualization, tracking, and procedure time with such active devices compared with passive guidewires. Clinical stents such as those used here are too short to heat at 1.5T.[54] We have found that the combination of active guidewire and Gd-DTPA–filled angioplasty balloon provided excellent imaging of devices and aortic wall lesions.

Conclusions

We have demonstrated preclinical safety and feasibility of wholly MRI-guided stent delivery for aortic coarctation. We used commercially available catheter devices. MRI provided satisfactory imaging for device tracking, navigation, stent deployment, accurate hemodynamic assessment, and assessment of stent apposition. Moreover, MRI provided immediate information about aortic rupture that may not have been available with conventional XRF. Freedom from ionizing radiation and superior image guidance are potentially important advantages, particularly in children.

Supplementary Material

Refer to Web version on PubMed Central for supplementary material.

References

1. Hamdan MA, Maheshwari S, Fahey JT, Hellenbrand WE. Endovascular stents for coarctation of the aorta: initial results and intermediate-term follow-up. J Am Coll Cardiol 2001;38:1518–1523. [PubMed: 11691533]

2. Slack MC. The role of stenting in coarctation of the aorta. Prog Pediatr Cardiol 2001;14:45–57.

3. Cheatham JP. Stenting of coarctation of the aorta. Catheter Cardiovasc Interv 2001;54:112–125. [PubMed: 11553960]

4. Rickers C, Jerosch-Herold M, Hu X, Murthy N, Wang X, Kong H, Seethamraju RT, Weil J, Wilke NM. Magnetic resonance image–guided transcatheter closure of atrial septal defects. Circulation 2003;107:132–138. [PubMed: 12515755]

5. Buecker A, Spuentrup E, Grabitz R, Freudenthal F, Muehler EG, Schaeffter T, van Vaals JJ, Gunther RW. Magnetic resonance–guided placement of atrial septal closure device in animal model of patent foramen ovale. Circulation 2002;106:511–515. [PubMed: 12135954]

6. Schalla S, Saeed M, Higgins CB, Martin A, Weber O, Moore P. Magnetic resonance–guided cardiac catheterization in a swine model of atrial septal defect. Circulation 2003;108:1865–1870. [PubMed: 14517162]

7. Kuehne T, Saeed M, Higgins CB, Gleason K, Krombach GA, Weber OM, Martin AJ, Turner D, Teitel D, Moore P. Endovascular stents in pulmonary valve and artery in swine: feasibility study of MR imaging-guided deployment and postinterventional assessment. Radiology 2003;226:475–481. [PubMed: 12563142]

8. Serfaty JM, Yang X, Foo TK, Kumar A, Derbyshire A, Atalar E. MRI-guided coronary catheterization and PTCA: a feasibility study on a dog model. Magn Reson Med 2003;49:258–263. [PubMed: 12541245]

9. Dick AJ, Guttman MA, Raman VK, Peters DC, Pessanha BS, Hill JM, Smith S, Scott G, McVeigh ER, Lederman RJ. Magnetic resonance fluoroscopy allows targeted delivery of mesenchymal stem cells to infarct borders in swine. Circulation 2003;108:2899–2904. [PubMed: 14656911]

10. Raman VK, Karmarkar PV, Guttman MA, Dick AJ, Peters DC, Ozturk C, Pessanha BS, Thompson RB, Raval AN, Desilva R, Aviles RJ, Atalar E, McVeigh ER, Lederman RJ. Real-time magnetic resonance-guided endovascular repair of experimental abdominal aortic aneurysm in swine. J Am Coll Cardiol 2005;45:2069–2077. [PubMed: 15963411]

11. Spuentrup E, Ruebben A, Schaeffter T, Manning WJ, Gunther RW, Buecker A. Magnetic resonance–guided coronary artery stent placement in a swine model. Circulation 2002;105:874–879. [PubMed: 11854130]

12. Strother CM, Unal O, Frayne R, Turk A, Omary R, Korosec FR, Mistretta CA. Endovascular treatment of experimental canine aneurysms: feasibility with MR imaging guidance. Radiology 2000;215:516–519. [PubMed: 10796934]

13. Manke C, Nitz WR, Djavidani B, Strotzer M, Lenhart M, Volk M, Feuerbach S, Link J. MR imaging–guided stent placement in iliac arterial stenoses: a feasibility study. Radiology 2001;219:527–534. [PubMed: 11323483]

14. Paetzel C, Zorger N, Bachthaler M, Volk M, Seitz J, Herold T, Feuerbach S, Lenhart M, Nitz WR. Feasibility of MR-guided angioplasty of femoral artery stenoses using real-time imaging and intraarterial contrast-enhanced MR angiography. Rofo 2004;176:1232–1236. [PubMed: 15346256]

15. Bucker A, Neuerburg JM, Adam GB, Glowinski A, Schaeffter T, Rasche V, van Vaals JJ, Gunther RW. Real-time MR guidance for inferior vena cava filter placement in an animal model. J Vasc Interv Radiol 2001;12:753–756. [PubMed: 11389228]

16. Buecker A, Adam GB, Neuerburg JM, Kinzel S, Glowinski A, Schaeffter T, Rasche V, van Vaals JJ, Guenther RW. Simultaneous real-time visualization of the catheter tip and vascular anatomy for MR-guided PTA of iliac arteries in an animal model. J Magn Reson Imaging 2002;16:201–208. [PubMed: 12203769]

17. Omary RA, Frayne R, Unal O, Warner T, Korosec FR, Mistretta CA, Strother CM, Grist TM. MR-guided angioplasty of renal artery stenosis in a pig model: a feasibility study. J Vasc Interv Radiol 2000;11:373–381. [PubMed: 10735435]

18. Bartels LW, Bos C, van Der Weide R, Smits HF, Bakker CJ, Viergever MA. Placement of an inferior vena cava filter in a pig guided by high-resolution MR fluoroscopy at 1.5 T. J Magn Reson Imaging 2000;12:599–605. [PubMed: 11042643]

19. Kee ST, Rhee JS, Butts K, Daniel B, Pauly J, Kerr A, O'Sullivan GJ, Sze DY, Razavi MK, Semba CP, Herfkens RJ, Dake MD. 1999 Gary J. Becker Young Investigator Award: MR-guided transjugular porto-systemic shunt placement in a swine model. J Vasc Interv Radiol 1999;10:529–535. [PubMed: 10357476]

20. Kuehne T, Yilmaz S, Meinus C, Moore P, Saeed M, Weber O, Higgins CB, Blank T, Elsaesser E, Schnackenburg B, Ewert P, Lange PE, Nagel E. Magnetic resonance imaging–guided transcatheter implantation of a prosthetic valve in aortic valve position: feasibility study in swine. J Am Coll Cardiol 2004;44:2247–2249. [PubMed: 15582324]

21. Razavi R, Hill DL, Keevil SF, Miquel ME, Muthurangu V, Hegde S, Rhode K, Barnett M, van Vaals J, Hawkes DJ, Baker E. Cardiac catheterisation guided by MRI in children and adults with congenital heart disease. Lancet 2003;362:1877–1882. [PubMed: 14667742]

22. Lock JE, Niemi T, Burke BA, Einzig S, Castaneda-Zuniga WR. Transcutaneous angioplasty of experimental aortic coarctation. Circulation 1982;66:1280–1286. [PubMed: 6216025]

23. Dick AJ, Raman VK, Raval AN, Guttman MA, Thompson RB, Ozturk C, Peters DC, Stine AM, Wright VJ, Schenke WH, Lederman RJ. Invasive human magnetic resonance imaging during

angioplasty: feasibility in a combined XMR suite. Catheter Cardiovasc Interv 2005;64:265–274. [PubMed: 15736247]

24. Guttman MA, McVeigh ER. Techniques for fast stereoscopic MRI. Magn Reson Med 2001;46:317–323. [PubMed: 11477636]

25. Guttman MA, Lederman RJ, Sorger JM, McVeigh ER. Real-time volume rendered MRI for interventional guidance. J Cardiovasc Magn Reson 2002;4:431–442. [PubMed: 12549231]

26. Konings MK, Bartels LW, Smits HF, Bakker CJ. Heating around intravascular guidewires by resonating RF waves. J Magn Reson Imaging 2000;12:79–85. [PubMed: 10931567]

27. Wang Y, Truong TN, Yen C, Bilecen D, Watts R, Trost DW, Prince MR. Quantitative evaluation of susceptibility and shielding effects of nitinol, platinum, cobalt-alloy, and stainless steel stents. Magn Reson Med 2003;49:972–976. [PubMed: 12704782]

28. *Heart Disease and Stroke Statistics: 2004 Update* Dallas, Tex: American Heart Association; 2003.

29. Brewer LA 3rd, Fosburg RG, Mulder GA, Verska JJ. Spinal cord complications following surgery for coarctation of the aorta: a study of 66 cases. J Thorac Cardiovasc Surg 1972;64:368–381. [PubMed: 5054875]

30. Kappetein AP, Zwinderman AH, Bogers AJ, Rohmer J, Huysmans HA. More than thirty-five years of coarctation repair: an unexpected high relapse rate. J Thorac Cardiovasc Surg 1994;107:87–95. [PubMed: 8283924]

31. Allen HD, Beekman RH 3rd, Garson A Jr, Hijazi ZM, Mullins C, O'Laughlin MP, Taubert KA. Pediatric therapeutic cardiac catheterization: a statement for healthcare professionals from the Council on Cardiovascular Disease in the Young, American Heart Association. Circulation 1998;97:609–625. [PubMed: 9494035]

32. Suarez de Lezo J, Pan M, Romero M, Medina A, Segura J, Lafuente M, Pavlovic D, Hernandez E, Melian F, Espada J. Immediate and follow-up findings after stent treatment for severe coarctation of aorta. Am J Cardiol 1999;83:400–406. [PubMed: 10072232]

33. Ebeid MR, Prieto LR, Latson LA. Use of balloon-expandable stents for coarctation of the aorta: initial results and intermediate-term follow-up. J Am Coll Cardiol 1997;30:1847–1852. [PubMed: 9385917]

34. Korkola SJ, Tchervenkov CI, Shum-Tim D, Roy N. Aortic rupture after stenting of a native coarctation in an adult. Ann Thorac Surg 2002;74:936. [PubMed: 12238877]

35. Ward KE. Complications of balloon coarctation angioplasty. Prog Pediatr Cardiol 2001;14:59–71.

36. American Academy of Pediatrics, Committee on Environmental Health. Risk of ionizing radiation exposure to children: a subject review. Pediatrics 1998;101:717–719. [PubMed: 9521965]

37. Raissaki M. Pediatric radiation protection. Eur Radiol Suppl 2004;14:74–83.

38. Committee on the Biological Effects of Ionizing Radiation BoRER, Commission on Life Sciences, National Research Council. *Health Effects of Exposure to Low Levels of Ionizing Radiation, BEIR V* Washington, DC: National Academy Press; 1990.

39. Brenner D, Elliston C, Hall E, Berdon W. Estimated risks of radiation-induced fatal cancer from pediatric CT. AJR Am J Roentgenol 2001;176:289–296. [PubMed: 11159059]

40. Infante-Rivarde C, Mathonnet G, Sinnet D. Risk of childhood leukemia associated with diagnostic irradiation and polymorphisms in DNA repair genes. Environ Health Perspect 2000;108:495–498. [PubMed: 10856021]

41. McLaughlin JR, Kreiger N, Sloan MP, Benson LN, Hilditch S, Clarke EA. An historical cohort study of cardiac catheterization during childhood and the risk of cancer. Int J Epidemiol 1993;22:584–591. [PubMed: 8225729]

42. Spengler RF, Cook DH, Clarke EA, Olley PM, Newman AM. Cancer mortality following cardiac catheterization: a preliminary follow-up study on 4,891 irradiated children. Pediatrics 1983;71:235–239. [PubMed: 6823426]

43. Modan B, Keinan L, Blumstein T, Sadetzki S. Cancer following cardiac catheterization in childhood. Int J Epidemiol 2000;29:424–428. [PubMed: 10869313]

44. Martin EC, Olson AP, Steeg CN, Casarella WJ. Radiation exposure to the pediatric patient during cardiac catheterization and angiocardiography: emphasis on the thyroid gland. Circulation 1981;64:153–158. [PubMed: 7237713]

45. Wu JR, Huang TY, Wu DK, Hsu PC, Weng PS. Radiation exposure of pediatric patients and physicians during cardiac catheterization and balloon pulmonary valvuloplasty. Am J Cardiol 1991;68:221–225. [PubMed: 2063785]

46. Berrington de Gonzalez A, Darby S. Risk of cancer from diagnostic X-rays: estimates for the UK and 14 other countries. Lancet 2004;363:345–351. [PubMed: 15070562]

47. Waldman JD, Rummerfield PS, Gilpin EA, Kirkpatrick SE. Radiation exposure to the child during cardiac catheterization. Circulation 1981;64:158–163. [PubMed: 7237714]

48. Moore JD, Shim D, Sweet J, Arheart KL, Beekman RH 3rd. Radiation exposure to children during coil occlusion of the patent ductus arteriosus. Catheter Cardiovasc Interv 1999;47:449–454. [PubMed: 10470475]

49. Boothroyd A, McDonald E, Moores BM, Sluming V, Carty H. Radiation exposure to children during cardiac catheterization. Br J Radiol 1997;70:180–185. [PubMed: 9135445]

50. Rees S, Somerville J, Ward C, Martinez J, Mohiaddin RH, Underwood R, Longmore DB. Coarctation of the aorta: MR imaging in late postoperative assessment. Radiology 1989;173:499–502. [PubMed: 2798882]

51. Nielsen JC, Powell AJ, Gauvreau K, Marcus EN, Prakash A, Geva T. Magnetic resonance imaging predictors of coarctation severity. Circulation 2005;111:622–628. [PubMed: 15699283]

52. Oshinski JN, Parks WJ, Markou CP, Bergman HL, Larson BE, Ku DN, Mukundan S Jr, Pettigrew RI. Improved measurement of pressure gradients in aortic coarctation by magnetic resonance imaging. J Am Coll Cardiol 1996;28:1818–1826. [PubMed: 8962572]

53. Liu CY, Farahani K, Lu DS, Duckwiler G, Oppelt A. Safety of MRI-guided endovascular guidewire applications. J Magn Reson Imaging 2000;12:75–78. [PubMed: 10931566]

54. Shellock FG, Shellock VJ. Metallic stents: evaluation of MR imaging safety. AJR Am J Roentgenol 1999;173:543–547. [PubMed: 10470877]
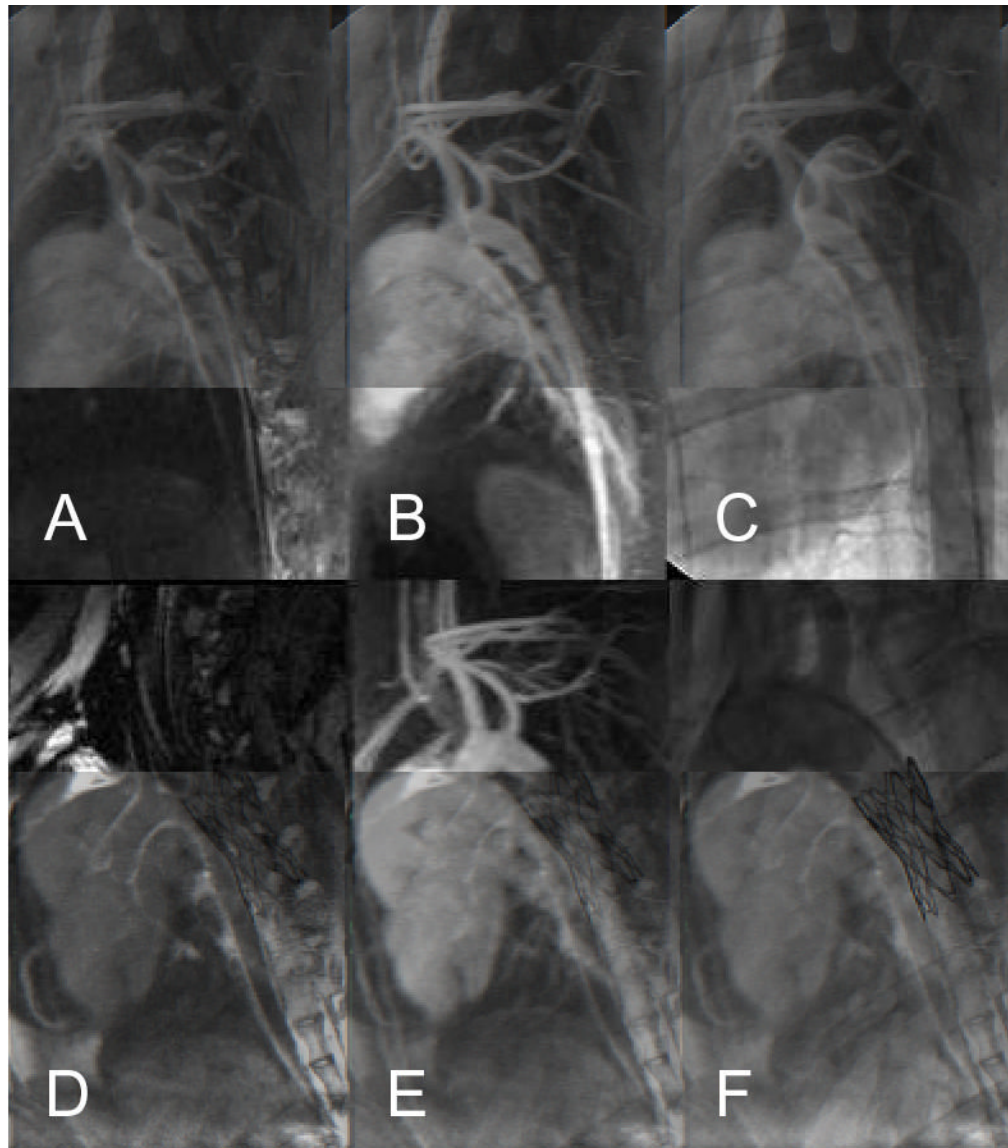
Figure 1.
Surgically created aortic coarctation in swine before (A–C) and after (D, E) stenting. A, D,
Black-blood DIR-FSE MRI. B, E, Contrast-enhanced MRA. C, F, Radiocontrast angiography.
Stent-related shielding artifact obliterates contrast in stent lumen (E). Scalloped appearance of
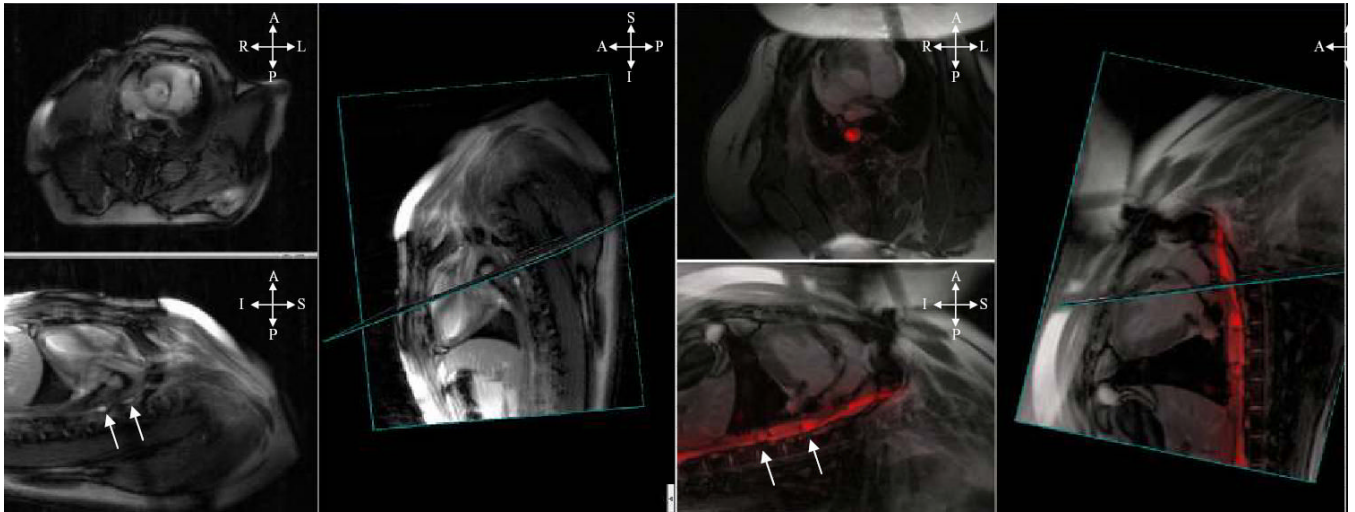aortic wall from apposed stent (D).

Figure 2.
rtMRI multislice axial (top left), sagittal (bottom left), and 3D-rendered (right) display of stent delivery across aortic coarctation. Passive (A) and active (B) guidewire tracking are compared. Dumbbell-shaped balloon carrying centrally crimped stent (white arrows) can be seen in both approaches; however, wire is much more clearly visible with active guidewire. S indicates superior; I, inferior; A, anterior; and P, posterior.
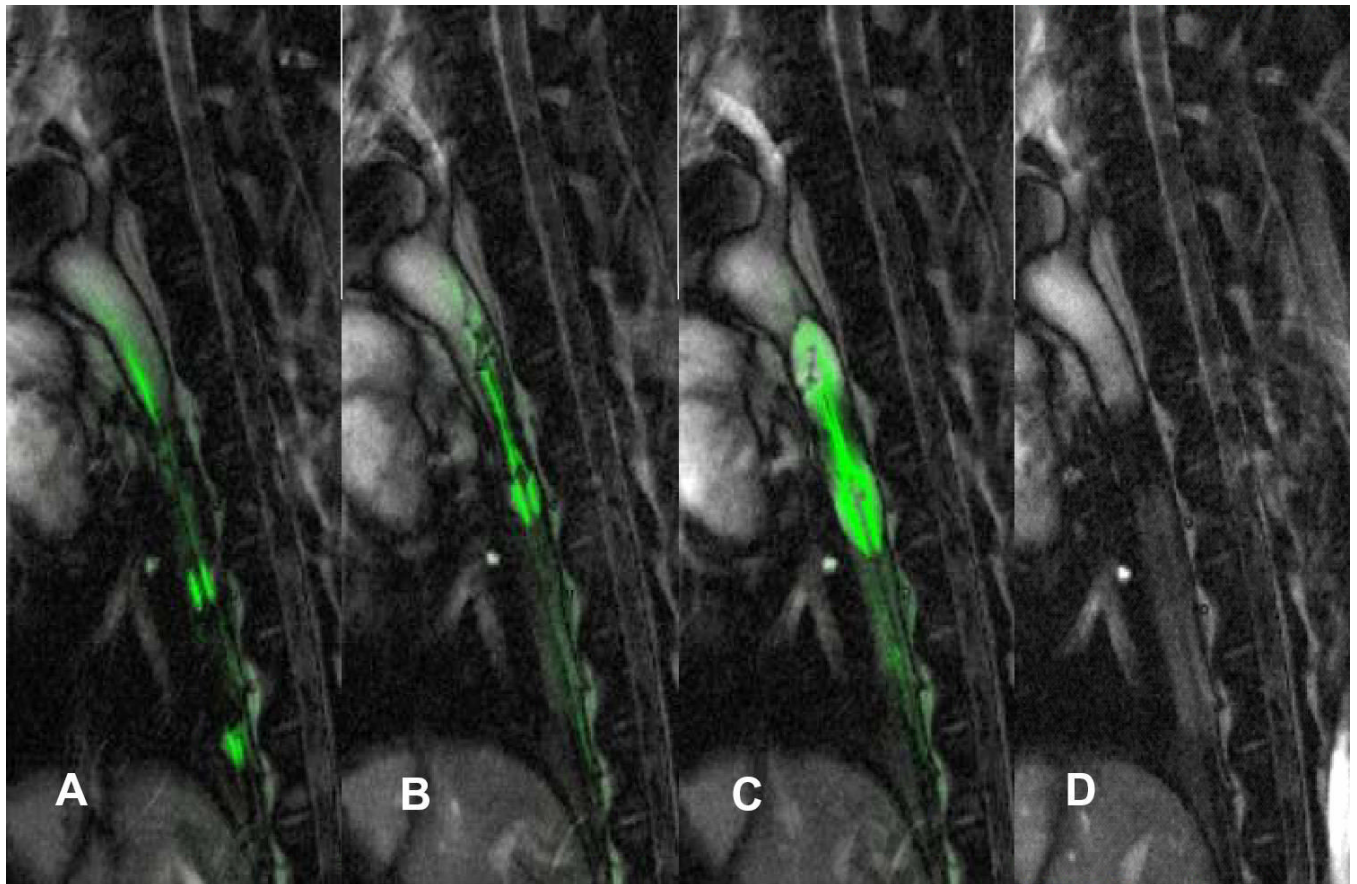
Figure 3.
Stent delivery sequence. A, Advancing balloon/stent over active guidewire. Also see Data Supplement Movie I. B, Positioning into coarctation. Also see Data Supplement Movie II. C, Balloon inflation. D, Shielding artifact darkens aorta after balloon and guidewire are withdrawn.
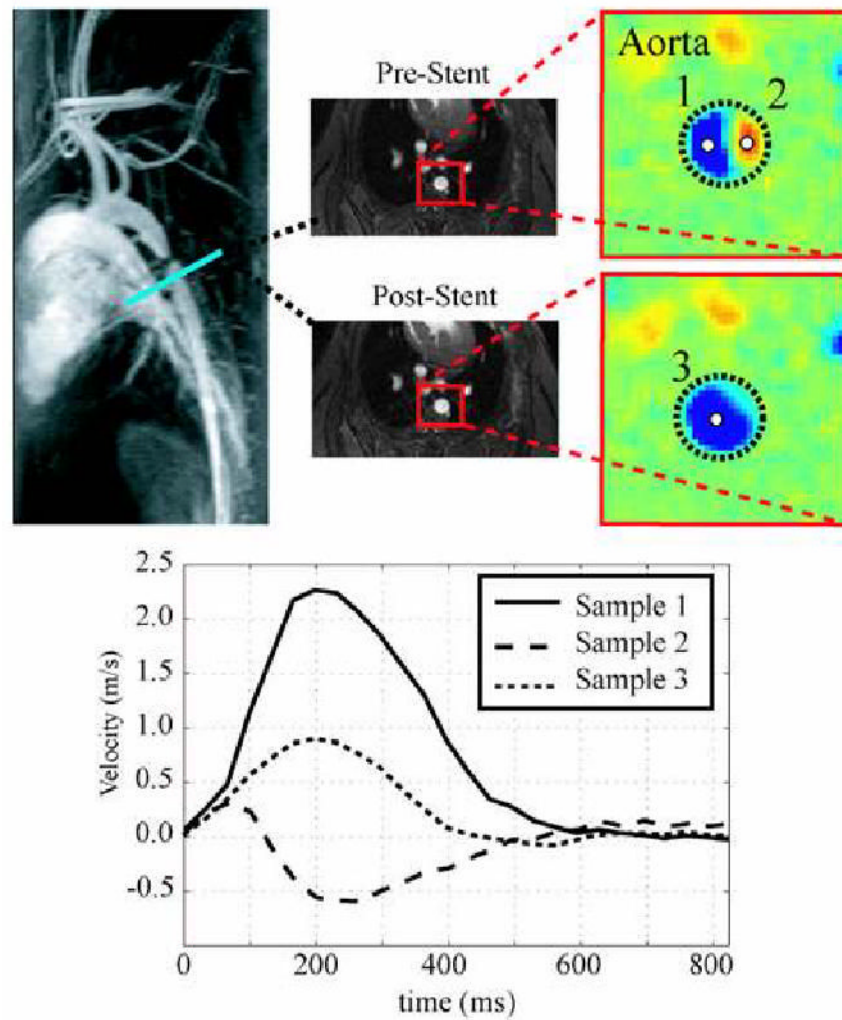
Figure 4.
Velocity map before and after stenting through plane indicated by blue line. Aortic cross sections are displayed as color maps during systole. Sample 1 shows jet acceleration from coarctation lesion; sample 2, flow reversal from turbulent blood flow; and sample 3, restoration of laminar flow with minimal blood acceleration after stenting.
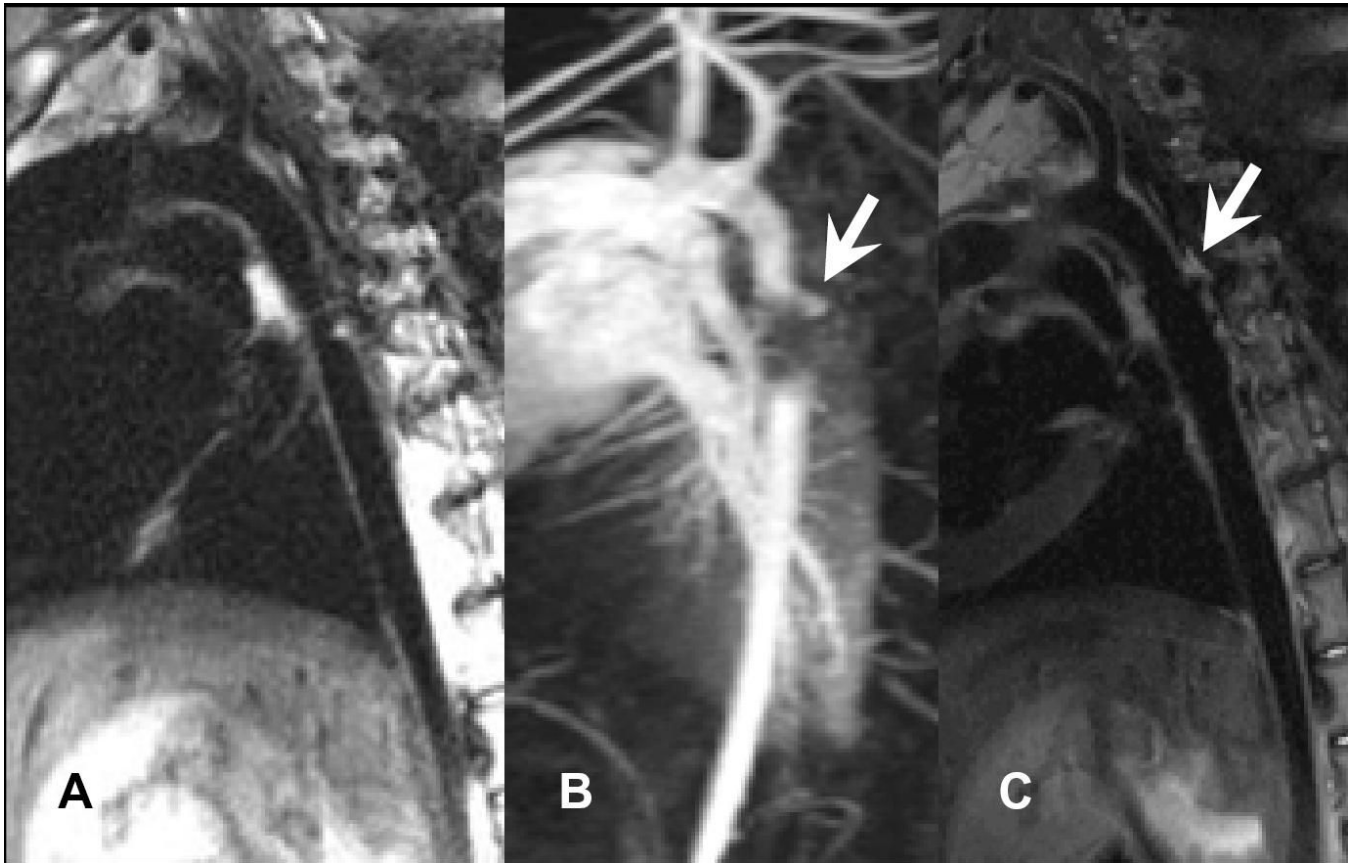
Figure 5.
Early detection of aortic perforation. A, DIR-FSE image of coarctation at before stenting. B, Contrast exit at superior edge of stent (arrow). C, DIR-FSE shows apposed oversized stent with blood accumulation along aortic wall (arrow).
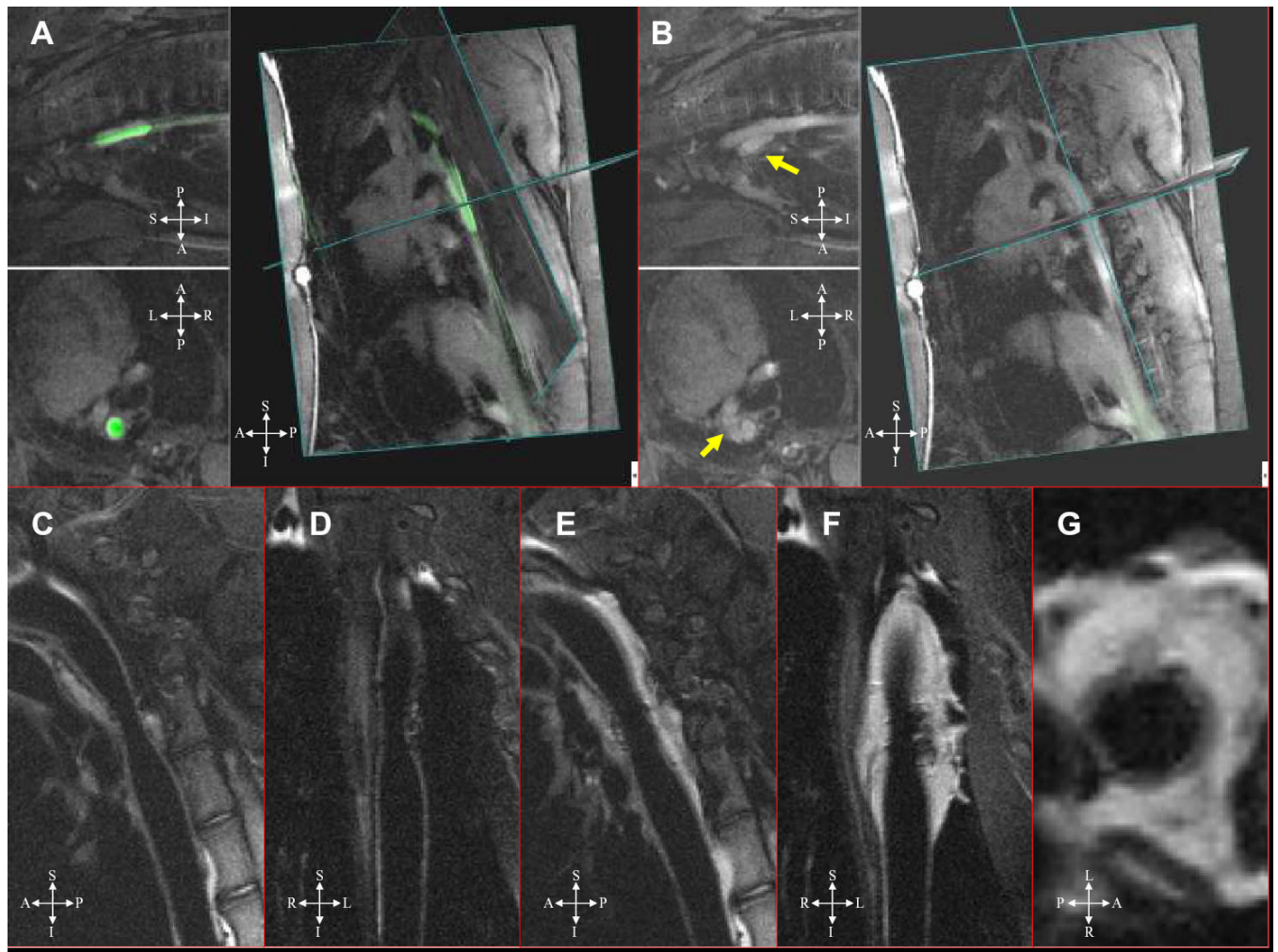
Figure 6.
Intentional aortic rupture. A, Simultaneous coronal (top left), axial (bottom left), and sagittal slices displayed and 3D rendered (right). Active wire is across coarctation (green), and oversized balloon is inflated. B, During continuous rtMRI, periaortic hematoma is evident immediately (arrows). DIR-FSE images before (C, D) and after (E, G) intentional rupture. Extravasation appears white. Abbreviations as in Figure 2. Also see Data Supplement Movie III.
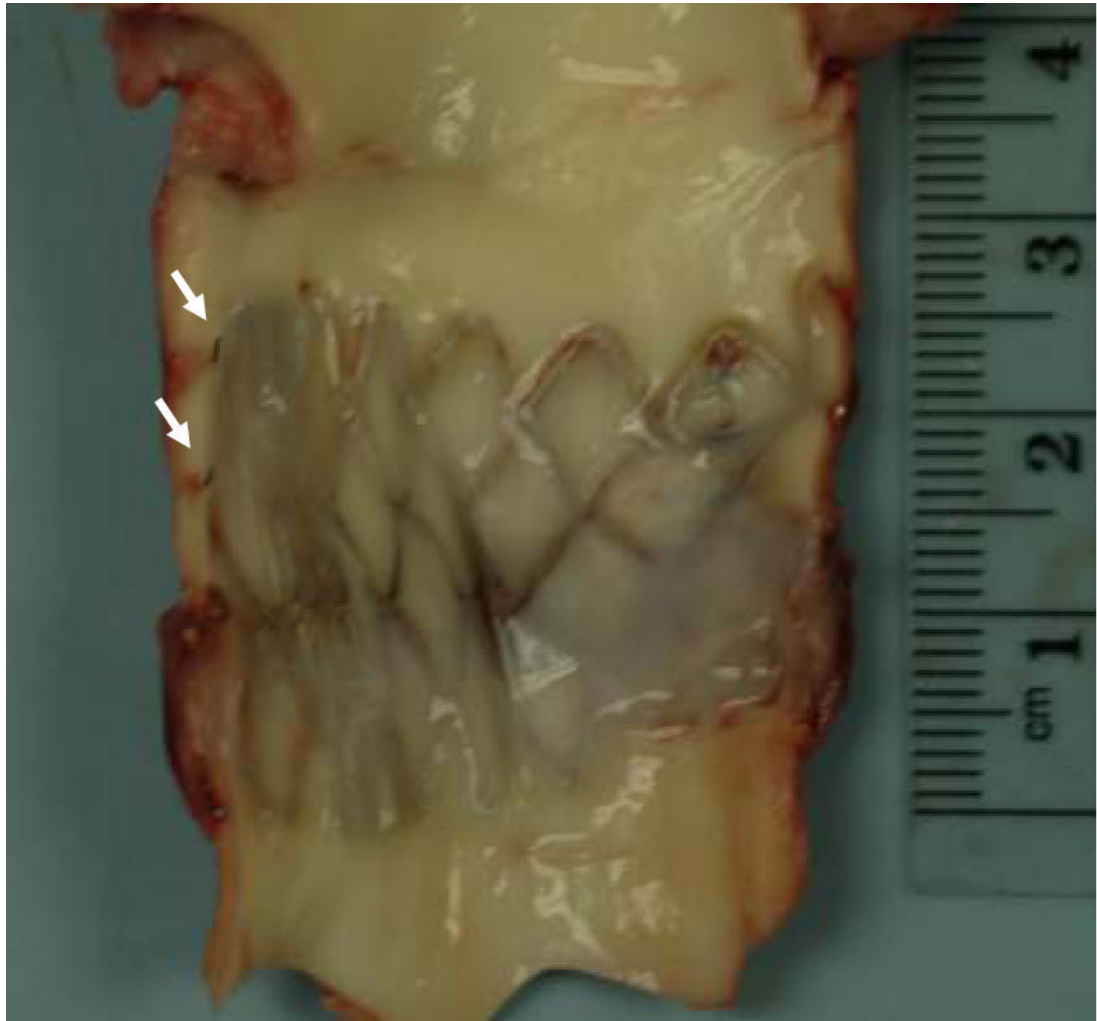
Figure 7.
Representative necropsy specimen 66 days after stent deployment. Sutures used to create coarctation are visible (arrows). Stent struts are fully apposed to wall and fully endothelialized.